Energy and Structure of the M2 Helix in Acetylcholine Receptor-Channel Gating

Archana Jha, Prasad Purohit, and Anthony Auerbach*
Department of Physiology and Biophysics, State University of New York, Buffalo, New York

ABSTRACT We studied single-channel currents from neuromuscular acetylcholine receptor-channels with mutations in the pore-lining, M2 helix of the ε-subunit. Three parameters were quantified: 1), the diliganded gating equilibrium constant (E_2), which reflects the energy difference between **C**(losed) and **O**(pen) conformations; 2), the correlation between the opening rate constant and E_2 on a log-log scale (Φ), which illuminates the energy character of the residue (**C**- versus **O**-like) within the **C** $\leftrightarrow$ **O** isomerization process; and 3), the open-channel current amplitude (i_0), which reports whether a mutation alters the energetics of ion permeation. The largest E_2 changes were observed in the cytoplasmic half of εM2 (5′, 9′, 12′, 13′, and 16′), with smaller changes apparent for residues $\geq$17′. Φ was ~0.54 for most εM2 residues, but was ~0.32 at the positions that had largest E_2 changes. An arginine substitution reduced i_0 significantly at six positions, with the magnitude of the reduction increasing, 16′ $\rightarrow$ 2′. The measurements suggest that the 9′, 12′, and 13′ residues experience large and late free-energy changes in the channel-opening process. We speculate that in the gating isomerization the pore-facing residues $>$6′ and $<$16′ experience multiple energy perturbations associated with changes in protein structure and, perhaps, hydration.

INTRODUCTION

Nicotinic acetylcholine receptor-channels (AChRs) mediate synaptic transmission between vertebrate nerve and muscle (1,2). The **C** $\leftrightarrow$ **O** ''gating'' isomerization of AChRs involves both a low $\leftrightarrow$ high affinity change for agonists at two transmitter binding sites and a low $\leftrightarrow$ high conductance change for ions through the pore. The transmitter binding sites are located in the extracellular domain of the protein, far (~50 Å) from the narrowest part of the ion permeation pathway. We, and others, seek to understand the changes in structure and energy that couple agonist affinity and conductance in this ~300 kD, five-subunit allosteric membrane protein.

Adult neuromuscular AChRs have five subunits: two α1 and one each of β, δ, and ε (3,4). The ε-subunit is located between the two α-subunits. One M2 transmembrane segment from each subunit lines the pore. Atomic-resolution structures are available for three members of the pentameric receptor-channel family. There is a 4 Å, cryo-electron microscopy model of unliganded native *Torpedo* AChRs (nAChR-*Tm* (5)) and x-ray models of the related prokaryotic and homomeric proteins ELIC (3.3 Å (6)) and GLIC (2.9 Å (7) and 3.1 Å (8)). These structural models can be used to interpret the gating free-energy changes caused by mutations. Here, we report the kinetics and amplitudes of single-channel currents of 140 mutations of 26 different residues of the mouse AChR εM2 helix.

The diliganded gating equilibrium constant (E_2) is the ratio of the diliganded, forward **C** $\rightarrow$ **O** opening (f_2) and backward **C** $\leftarrow$ **O** closing (b_2) rate constant. The free-energy difference between the stable **C** and **O** end states is proportional to the natural logarithm of the equilibrium constant ($\Delta G^{C\text{-}O} = -RT\ln E_2$, where R is the gas constant and T is the absolute temperature), so a mutation-induced change in E_2 indicates that the free-energy change caused by that side-chain substitution has a different magnitude in **C** versus **O**. Free energy is related to structure and dynamics, so such a difference suggests that during the gating process there is a change in the structure/dynamics of the mutated residue, its environment, or both. The measured energy changes pertain to the whole system, which includes the protein, lipids, ions, and water. Many mutations that are far from the transmitter binding site have been shown to change E_2 by a parallel change in the unliganded gating equilibrium constant rather than by a change in the **C** versus **O** ligand affinity ratio (9).

A second parameter that can be derived from the rate constants is Φ, the correlation between f_2 and E_2 on a log-log scale (the slope of the rate-equilibrium (R/E) plot). A mutation can change f_2 by changing the energy difference between **C** and the separating barrier, the prefactor, or both (10). Φ illuminates the fractional free energy of the perturbed residue within the transition pathway (**TP**) of the **C** $\rightarrow$ **O** isomerization, on a scale of 1 (**O**-like) to 0 (**C**-like). If the **TP** is defined only by a single structural intermediate, Φ is likely to reflect the fractional **C** versus **O** conformation of the mutated residue. If, however, the **TP** is a sequence of structural intermediates, then Φ can reflect the relative time within this chain when the mutated residue flips, essentially instantaneously and in an all-or-none fashion, between its **C** and **O** conformations (11).

A third useful single-channel measurement is the open-channel current amplitude, i_0. This parameter is a function of the reversal potential and conductance, which respectively reflect the type(s) and rate(s) of ions passing through the **O**-conformation pore. A mutation-induced change in i_0

Submitted September 16, 2008, and accepted for publication February 23, 2009.

*Correspondence: auerbach@buffalo.edu

Editor: Kenton J. Swartz.

0006-3495/09/05/4075/10 $2.00

doi: 10.1016/j.bpj.2009.02.030

therefore suggests that the side chain is able to interact energetically with the aqueous milieu of the open channel.

Below, we report measurements of E_2, Φ , and i_0, and discuss how they relate to the mechanism of $\mathbf{C} \leftrightarrow \mathbf{O}$ gating in the AChR M2 domain.

MATERIALS AND METHODS

A detailed account of the mutation, expression, and kinetic analysis methods used in this study is provided in Jha et al. (12). Except where noted, mutant ε-subunits were transiently expressed with mouse wild-type (WT) α-, β-, and δ-subunits in HEK cells, and single-channel currents were recorded in the cell-attached patch configuration at 23°C. The bath and pipette solutions were Dulbecco's phosphate-buffered saline (PBS) containing (in mM) 137 NaCl, 0.9 $CaCl_2$, 2.7 KCl, 1.5 KH_2PO_4, 0.5 $MgCl_2$, and 8.1 Na_2HPO_4 (pH 7.4). The currents were low-pass filtered at 20 kHz and digitized at a sampling frequency of 50 kHz. Agonist (acetylcholine or choline) was added only to the pipette solution. Choline was used to activate constructs in which E_2 was equal to or larger than that of the WT, and ACh was used to activate constructs in which E_2 was smaller than that of the WT. Kinetic analyses were done with the use of QUB software (www.qub.buffalo.edu). Clusters of individual-channel, $\mathbf{C} \leftrightarrow \mathbf{O}$ activity were selected so that the flanking, nonconducting intervals were $\geq$50 ms (t_{crit}).

We estimated f_2 and b_2 (after low-pass filtering to 10–12 kHz) from the idealized intracluster interval durations using a maximum likelihood algorithm (13) after imposing a dead time, typically 2.5 samples (50 μs). In our experiments E_2 (= f_2/b_2) pertains to the entire $\mathbf{C} \leftrightarrow \mathbf{O}$ isomerization and is therefore the product of the shut↔"flip" and "flip"↔open equilibrium constants (14,15). In some patches the rate constants were estimated by using a simple shut↔open model (because the log likelihood of the fit did not increase upon the addition of more shut or open states), whereas in others a second shut state was connected to the open state to accommodate a relatively rare and short-lived shut state associated with desensitization (16). For the unliganded gating equilibrium constant (E_0) measurements, a second open state was added to the kinetic scheme (see Fig. 4 and Results).

For the rate constant measurements, the agonist concentration was ~5 times the **C**-conformation equilibrium dissociation constant (K_d) of WT AChRs, that is, 500 μM ACh or 20 mM choline. At 500 μM the net association time for ACh is ~12 μs, so virtually all intervals (greater than the dead time) arose from diliganded AChRs. At 5× K_d the measured value of f_2 is ~70% of the correct value because of incomplete saturation of the binding sites (17). This error was assumed to be similar for all mutants and both agonists (12).

Except where noted, the potential of the patch pipette was +70 mV, which corresponds to a membrane potential of ~−100 mV. Variability in the cell potential in PBS creates some scatter in the measurements of both E_2 (~±20% in WT AChRs assuming a voltage sensitivity of 70 mV/e-fold change in b_2 (18)) and i_0 (~±1 pA in WT AChRs assuming a conductance of 70 pS). Current amplitudes were estimated at 30 μM ACh (i_0; ~7 pA in WT AChRs), where there was little channel block by the agonist, and at either 500 μM ACh or 20 mM choline (i_B) where unresolved channel block by the agonist was apparent. The amplitudes in Table S1 in the Supporting Material are the means for ~1000 open-channel intervals, each of which was estimated by using the SKM algorithm (19) without digital low-pass filtering. At 5× K_d the reduction in the current amplitude and increase in open channel noise caused by unresolved channel block by the agonist did not prevent detection of the gating transitions. The equilibrium dissociation constant for block ($K_{d\text{-}block}$) by ACh is ~1.9 mM in WT AChRs (20), and by choline it is ~12 mM for both WT (21) and for AChRs with a point mutation of the M2-9′ residue in the α-, ε-, or β-subunit (22). There is evidence that in WT AChRs agonist-blocked channels usually close before the agonist dissociates from the pore (21). We assumed that this was also true for the εM2 mutants, and accordingly used the following equation: $i_B \approx i_0/(1+[A]/K_{d\text{-}block})$. In WT AChRs $i_B \approx 5.5$ pA in 500 μM ACh, and $i_B \approx 2.6$ pA in 20 mM choline. We assumed that channel block slows the apparent closing rate constant to approximately the same degree that it reduces the current amplitude, so for each construct (examined at +70 mV pipette potential) the observed b_2 value was corrected using the following relationship: $b_2^{corrected} = b_2^{observed}(i_0/i_B)$. No correction for channel block was made for the patches examined at −70 mV pipette potential (13′AGN, 12′RL, 9′E, and 5′F).

In WT AChRs, desensitization mainly proceeds from the diliganded-**O** state (20), and we assumed that this was also true for the εM2 mutants. At low agonist concentration the open-channel lifetime (τ_o) is approximately the inverse of b_2 plus the rate constant for desensitization from the diliganded **O** conformation (k_{+D}) (23). In WT AChRs activated by ACh, and in some spontaneously active mutants (9), k_{+D} (~20 s^{-1}) is $<<b_2$ (~1700 s^{-1}) (23) and can be ignored. However, for some εM2 mutants τ_o (at a pipette potential of +70 mV) was $\geq$10 ms, raising the possibility that for these mutants desensitization may have contributed significantly to the b_2 estimate. To test for the possibility that desensitization from diliganded-**O** may have influenced some b_2 estimates, we coexpressed some εM2 mutants (Table S2) with α-subunits having a distant background mutation (αT422V, in M4). This mutation by itself decreases f_2 by 4.6-fold and increases b_2 by 5.3-fold (24) ($\Phi = 0.48$). We tested (at +70 mV pipette potential) whether this background mutation was independent energetically from one εM2 mutation, εA262F (10′), where on a WT background $f_2 = 609$ s^{-1} and $b_2 = 231$ s^{-1} (Table S1). The αT422V mutation decreased f_2 and increased b_2, each by ~4.5-fold (135 s^{-1} and 1029 s^{-1}, respectively; means of three patches; data not shown). This result indicates that the αT422V background mutation is approximately independent energetically from the εM2-10′ mutation. Even on this background, five εM2 mutants (I5′F, T12′R, and V13′AGN) still had $\tau_o \geq 10$ ms. For these, we additionally changed the pipette potential to −70 mV, a perturbation that alone in WT AChRs causes a ~10-fold increase in b_2 (18). We measured the effect of this depolarization on the εA262F+αT422V construct ($n = 2$ patches; data not shown). The result was $f_2 = 88$ s^{-1} and $b_2 = 9937$ s^{-1}, which is, relative to the +70 mV condition, a 1.5-fold decrease and a 9.7-fold increase, respectively. This result indicates that the voltage perturbation is approximately independent energetically from the εM2-10′ and αT422V mutations. The raw and background/voltage-corrected rate constants are reported in Table S2.

The change in end-state energy (kcal/mol) is $\Delta\Delta G^{\mathbf{O\text{-}C}} = 0.59*\ln(E_2^{mutant}/E_2^{reference})$. For each residue, we calculated the energy change for 1), each side-chain substitution (mutant in reference to the WT); and 2), the maximal range of E_2 for all substitutions at that position (largest E_2 in reference to the smallest E_2). There are two α-subunits per AChR, and hybrid analyses indicate that in αM2 (positions 9′, 17′, and 23′) the energy change magnitudes are approximately equivalent in each (22,25). Therefore, to compare $\Delta\Delta G^{\mathbf{O\text{-}C}}$ values between single ε- and α-subunits, the energy difference change for each αM2 residue was assumed to be half of the value observed in the whole AChR.

Φ was estimated as the slope of a linear fit to the R/E curve, which is a plot of log f_2 versus log E_2. Points in the R/E plots represent the mean of all the patches for each mutant construct. The WT values used to normalize f_2 and E_2 were 120 s^{-1} and 0.046 for choline (22) or 48,000 s^{-1} and 28.2 for ACh (26).

The K_d for acetylcholine was estimated from cluster interval durations obtained at different ACh concentrations (see Fig. 4). The two agonist-binding sites were assumed to be equivalent and independent (27), and the interval durations at all concentrations were fitted together by using a kinetic model that had four rate constants as free parameters: single-site association (k_+, scaled by the agonist concentration), single-site dissociation (k_-), f_2, and b_2.

E_0 was measured as described elsewhere (9). The **C/O** equilibrium dissociation constant ratio is equal to $\sqrt{(E_2/E_0)}$; a mutation that produces the same fold-change in E_2 and E_0 therefore has no effect on this ratio.

We could not determine E_2, Φ, and i_0 for some constructs. For T2′R, I5′R, and A10′R, the current amplitude was too small to allow the reliable detection of gating interval durations, and for I5′K, L9′R, A10′K, and I18′R, the currents had multiple levels (the current amplitudes shown in Table S1 and Fig. 5 pertain to the smallest level, except for 18′, for which no clear levels

could be estimated). For N6′G, N6′R, and V13′R, no open-channel currents were detected (five patches each, ~15 min/patch), either because there was no (or little) expression, the expressed AChRs rarely adopted an ion-conducting conformation, the open-channel currents were too small or brief to be detected by our instrument, or perhaps because of some combination thereof.

The limitations of the above experimental methods should be kept in mind with regard to the interpretation of the results. First, the range-energy metric for the **C** versus **O** energy difference for each position was computed from the range of E_2 values observed for a few random side-chain substitutions. We cannot be sure that some untested substitutions, natural or unnatural, would not have significantly expanded this range and increased the energy estimate. The range-energy value is therefore a minimum estimate of the energy change experienced by a residue. Second, with regard to i_0, we did not measure the reversal potential for each mutant. It is therefore possible that a WT-like current amplitude reflects offsetting changes in conductance and reversal potential, generating a false-negative result. Also, the arginine side chain is large (~7 Å, extended) and has rotors that separate the guanidinium group from the protein backbone, so the exact location of the positive charge relative to the backbone cannot be pinpointed.

RESULTS

The amino acid sequence for mouse εM2 (cytoplasmic→extracellular, N→C, 1′→28′) is CTVSINV**LL**AQ**TVF**L FLIAQKI**P**ETSLS. In bold are the M2 positions that are completely (L8′, F14′, and P23′) or almost completely (L9′, T12′, and V13′) conserved among all mouse AChR subunits. In M2, only P23′ is conserved between ELIC, GLIC, and AChRs. In these three proteins the M2 side chains $\leq 17'$ are mostly hydrophobic, except for positions 2′ (mostly T or S) and 6′ (mostly S, N, or T).

Fig. 1 shows the range of the free-energy change as a function of M2 position in α and ε, calculated from the observed maximal and minimal E_2 values. This range-energy (Table 1) provides a metric by which energy changes realized in **C**↔**O** gating by different residues can be calibrated. In εM2 the three largest range-energy values were at positions 5′, 12′, and 13′, whereas in αM2 the three largest values were at 13′, 23′, and 26′. The conserved P23′ and outer ring (28) position Q20′ experience only a small range-energy change in the ε-subunit. In both α and ε the 2′ residue, which may form the narrowest region of the open AChR pore (29), and the 6′ residue show little energy change between **C** and **O**.

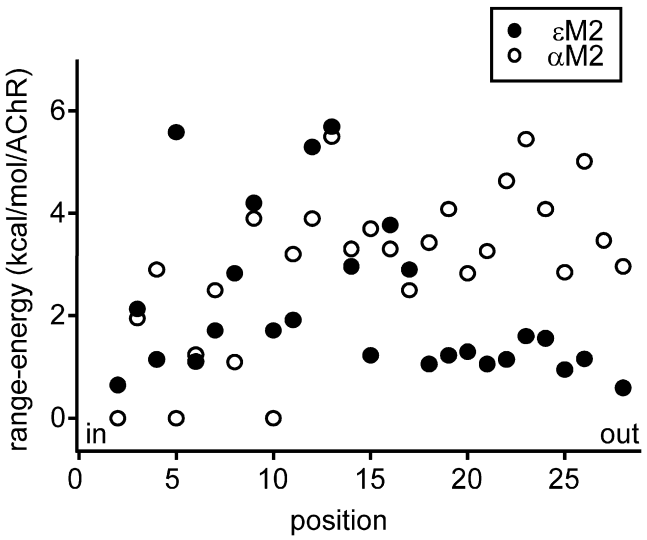

FIGURE 1 Gating energy changes in εM2 and αM2. Plot of the observed range of free-energy change for each M2 position. In the ε-subunit the four residues experiencing the largest energy changes were 5′, 9′, 12′, and 13′, whereas in the α-subunit they were 13′, 22′, 23′, and 26′.

TABLE 1 Functional properties of εM2 mutants, by position

Position	Mutation	E_2 Range(fold-change)	E_2 Energy (kcal/mol)	Φ (± SD)	i_0^R (pA)
T254(2′)	L,A,V,N	3	0.6	—	0.1
V255(3′)	R,A,S,D	37	2.1	0.56 (0.06)	4.5
S256(4′)	L,Y,N,G,C,R,D	7	1.1	—	7.5
I257(5′)	F,A	12767	5.6	0.33 (0.08)	0.5
N258 (6′)	D,T	7	1.1	—	NE
V259(7′)	R,E,A,D	18	1.7	0.58 (0.1)	1.6
L260(8′)	D,G,R	122	2.8	0.50 (0.1)	3.5
L261(9′)	G,E,F	1240	4.2	0.37 (0.1)	6.9
A262(10′)	F,Y,L,N	18	1.7	0.59 (0.05)	1.2
Q263(11′)	K,E,W	26	1.9	0.55 (0.04)	5
T264(12′)	R,L,A	7796	5.3	0.26 (0.08)	2
V265(13′)	N,G,A	15520	5.7	0.34 (0.07)	NE
F266(14′)	W,S,N,R,L	151	3.0	0.56 (0.07)	5.3
L267(15′)	D,F,W,A	8	1.2	—	3.9
F268(16′)	R,G,C,T,W	597	3.8	0.51 (0.06)	2.5
L269(17′)	F,T,R	179	2.9	0.52 (0.06)	7.7
I270(18′)	T,E,W,V	6	1.1	—	ND
A271(19′)	R,G,N,T	8	1.2	—	6.5
Q272(20′)	E,R,A,V,T	9	1.3	—	4.8
K273(21′)	T,E,A,R,V	6	1.1	—	6.4
I274(22′)	V,R,E,A	7	1.1	—	7.9
P275(23′)	R,E,A,V	15	1.6	0.51 (0.1)	7.9
E276 (24′)	D,H,V,R,T,K,I,A	14	1.6	0.56 (0.12)	4.7
T277 (25′)	G,R,Q,E,D,F,A	5	0.9	—	7.2
S278(26′)	E,R,V,W	7	1.2	—	7.2
S280(28′)	D,A,R,G	3	0.6	—	7.5

E_2 range is the ratio of the most extreme E_2 values at each position; E_2 energy is 0.59 times the natural logarithm of this ratio. Φ-Values were not estimated for positions where the fold-change in E_2 was ≤13-fold. i_0^R is the single-channel current amplitude of the arginine mutant. NE, no expression of functional channels; ND, no data because there was no clear single-channel current amplitude (see Fig. S1).

Fig. 2 shows the rate constants for εM2 mutants plotted in the form of R/E plots. The slope of this relationship cannot be estimated precisely when the range-energy is small (30), so we estimated Φ only for the 14 εM2 positions that showed a ≥1.5 kcal/mol range-energy (12.7-fold range in E_2). Fig. 3 *a* compares histograms of Φ-values for residues in εM2 and αM2 (22,25,31), and Fig. 3 *b* shows the Φ-values as a function of position. In ε, most Φ-values fall into a narrow range (0.50–0.59; 0.54 ± 0.03; mean ± SD), but at four positions (5′, 9′, 12′, and 13′) the Φ-values were smaller (0.32 ± 0.05). In αM2, most residues also had an intermediate Φ-value, with a mean ± SD (0.63 ± 0.06) and range (0.51–0.78) somewhat greater than in εM2. In the α-subunit, only the

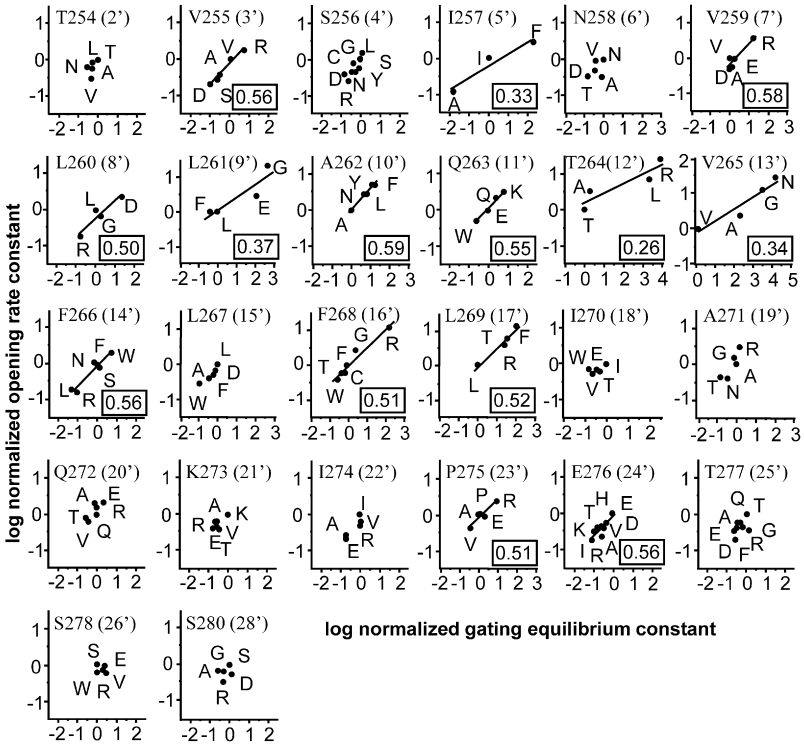

FIGURE 2 R/E plots of εM2 residues. In the rate-equilibrium free-energy relationships (R/E plots), a point is the average from multiple patches for that mutant (Table S1). The opening rate constants and equilibrium constants were normalized as mutant/WT (a positive value indicates a gain of function). The slope, Φ, is boxed (Table 1). Φ-values were estimated only for positions where the range-energy was ≥1.5 kcal/mol.

9′ and 12′ positions belonged to the low-Φ population. Using the interpretation that Φ reflects the relative timing of the gating free-energy change in the mutated side chain, this pattern suggests that most residues in εM2 and αM2 experience their **C** versus **O** energy change(s) approximately midway through the **TP** sequence, but that the low-Φ amino acids change free energy, on average, relatively later in the opening process.

We measured the ACh binding parameters for one εM2 mutant construct, E24′I, which reduced E_2 by 13.8-fold (Fig. 4 *a*). First, we measured the single-site association (k_+) and dissociation (k_-) rate constants for the **C** conformation, and from these calculated an equilibrium dissociation constant ($K_d = k_-/k_+$). In this mutant, k_+, k_-, and K_d (178 ± 10 $\mu M^{-1}s^{-1}$, 24,548 ± 1615 s^{-1}, 138 ± 18 μM, respectively; Fig. 4 *b*) were all similar to the WT values (167 $\mu M^{-1}s^{-1}$, 24,745 s^{-1}, 148 μM, respectively (32)). To determine whether this mutation changed the affinity of the **O** conformation, we also measured the unliganded gating equilibrium constant (E_0) of this mutant coexpressed on a triple mutant background (Fig. 4 *c*). The nonconducting intervals within E24′I unliganded clusters were described by one exponential, but the conducting intervals had a double exponential distribution. We used either of two kinetic schemes, $C \leftrightarrow O_1 \leftrightarrow O_2$ or $O_2 \leftrightarrow C \leftrightarrow O_1$, to estimate the unliganded gating rate constants f_0 and b_0. From the $C \leftrightarrow O_1$ rate constants, we calculate that relative to the triple-mutant background, the E24′I mutation decreased f_0 by fourfold and increased b_0 by 3.3-fold (first scheme), or decreased f_0 by 5.3-fold and increased b_0 by 3.7-fold (second scheme). Thus, the E24′I mutation decreases E_0 by 13.1-fold or 19.6-fold, neither of which is dissimilar from the 13.8 decrease in E_2. This observation indicates that this εM2 mutation does not substantially alter the **C/O** affinity ratio. Together, these two results indicate that E24′I does not substantially affect ACh binding to either the **C** or the **O** conformation. This observation is consistent with a previous study (9) showing that many mutations that are far from the transmitter binding sites, including four at εM2−13′, do not alter agonist-binding properties. We therefore assumed that all of the mutations we examined in εM2 altered E_2 by a parallel change in E_0.

Fig. 5 shows the consequences of εM2 point mutations on the single-channel current amplitude (i_0). Excluding R substitutions (Fig. 5, *top panel*), the average current amplitude of the mutants (6.8 ± 0.1 pA) was similar to that of the WT (~7 pA). There was a slight trend for the mutations in the cytoplasmic half of εM2 to decrease, and those in the extracellular half to increase, i_0. The linear fit (i_0 versus prime index) had a slope of 0.064 ± 0.012 and an intercept of 5.78 ± 0.27 pA. E or D side chains did not affect the current differently from the uncharged substitutions. Only small changes in i_0 were observed for 12 different mutations of the two charged εM2 residues K21′(AERTV) and E24′(ACHKITV). Substitution of a charged (R or E) or an uncharged (A, T, or V) side chain at the ''outer ring'' position εQ20′ did not substantially alter i_0.

Fig. 5 (*bottom panel*) shows i_0 for R substitutions at each εM2 position. We could not detect single-channel currents for the 6′R and 13′R constructs, perhaps because the open

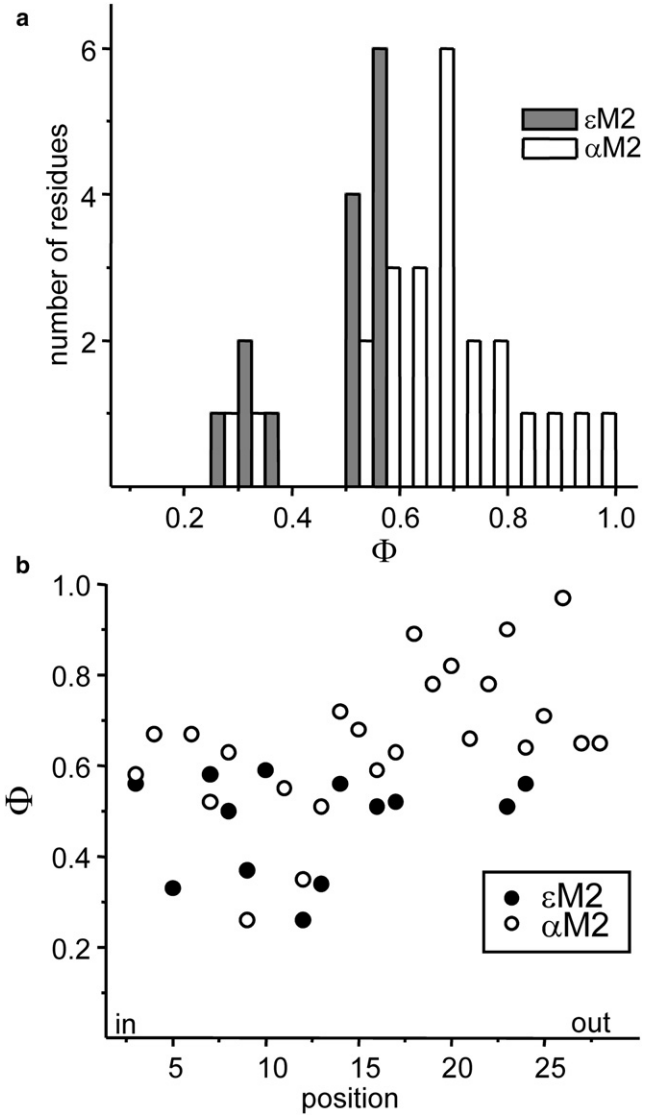

FIGURE 3 Φ-values for εM2 and αM2. (*a*) Histograms of residue Φ-values. Most εM2 residues have Φ ~ 0.54, but four (5′, 9′, 12′, 13′) have a value of ~0.32. αM2 has more high-Φ residues, as well as two with Φ ~ 0.32 (9′, 12′). (*b*) Plot of Φ-value by position. The high-Φ residues in αM2 are in the C-terminal ''cap'' region, and the low-Φ residues in both subunits are at positions ≤13′.

current was too small. Other possible explanations for this result are that the sojourns in conducting conformations were rare or brief, or that these constructs did not express on the cell surface. The i_0 value of the R mutants deviated significantly from the expected i_0 value (≥3 SD from the straight-line fit to the non-R substitution data) at six positions: 2′, 5′, 7′, 10′, 12′, and 16′. The magnitude of the deviation increased as the position of the R substitution approached the cytoplasmic limit of the helix. Although an R substitution at 9′ did not significantly reduce i_0, sublevel currents were apparent here (Fig. S1). Because only R substitutions significantly reduced the current amplitude, it is likely that the reductions in i_0 were caused by unfavorable energetic interactions of the guanidinium head group with permeating ions (at pH 7.4 the R side chain is likely protonated below 17′ (33)).

Considering the size of the R side chain, there is a reasonable correlation between the positions that show an attenuation of the current and those that face the lumen of the pore in nAChR-*Tm* (see Fig. 6). The increasing degree of current attenuation, 16′→2′ (which might reflect a gradient in diameter or dielectric constant), is consistent with a radial tilt of M2, but the possibility that 6′R and 13′R currents are tiny and the fact that the amplitude of 9′R was not attenuated do not fit neatly with this hypothesis. If the nAChR-*Tm* structure is **C**, these results are consistent with there being little or no rotation about the M2 helix axis between **C** and **O** conformations (33).

DISCUSSION

The estimates of the effects of mutations on E_2 and Φ provide information about the magnitude and relative timing of the free-energy changes in **C**↔**O** gating. Our task is to interpret these results using existing information regarding M2 structure and function to synthesize a plausible model for the energy and conformational changes in this helix within the AChR gating isomerization.

Fig. 1 shows the pattern of energy change in M2 in ε and α, as given by the range-energy metric for each position. In ε, residues in the extracellular, C-terminal ''cap'' of the helix experience little energy differences between **C** and **O**, whereas many residues below this point experience larger energy differences. This pattern is different from that in the α-subunit, where the largest energy changes occur in residues >17′, including the ring position 20′ and the conserved P23′ (25). This highlights the α-subunit M2 cap as an early, moving part of the AChR gating machine (8). The cap regions of δ and β have not been investigated in detail, so it remains to be determined whether this domain is important energetically only in the α-subunit.

We now focus on the mutational effects at M2 positions 2′–17′. The range-energy is a noisy, minimum estimate (see Materials and Methods), but at present it is the only metric we know of that can be used to compare quantitatively the gating free-energy changes experienced by different residues. In this region of M2, the number of positions where a range-energy has been estimated (based on ≥2 mutants) are 16 in α (22,25,31), 16 in ε, 10 in δ (30), and 1 in β (22). There was no clear modal distribution in the range-energy values for these 43 residues, so for classification purposes we categorized the top quartile (≥3.8 kcal/mol) as ''large'' and the second quartile (2.5–3.7 kcal/mol) as ''intermediate''. There were 14 residues that had a range-energy <1.5 kcal/mol, and we categorize these as being approximately isoenergetic between **C** and **O**.

Fig. 6 (*left*) displays the range-energy metric for M2 positions in the α-, ε-, and δ-subunits. In ε, five positions were

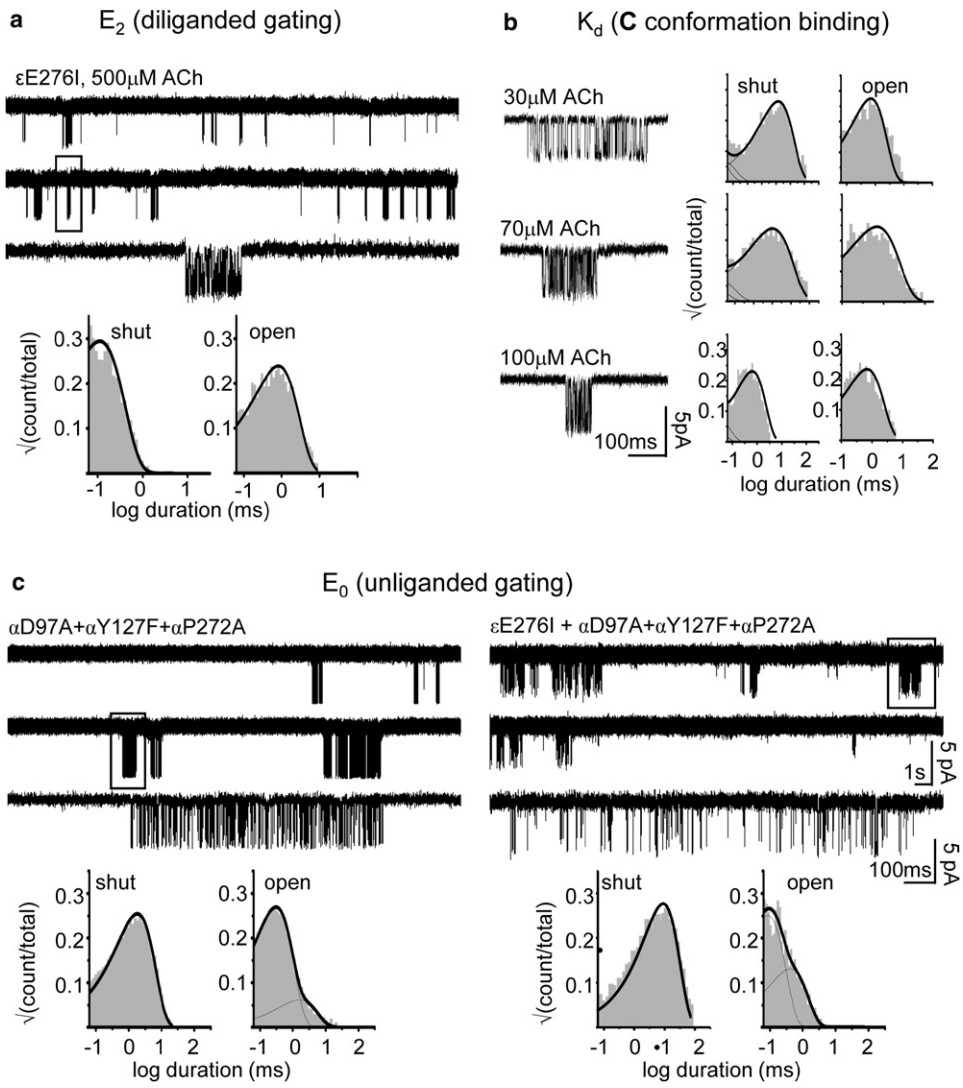

FIGURE 4 Binding and gating analyses of E24′I. (*a*) E_2 estimation. Top: Upper two traces are low time-resolution currents; bottom trace is expanded view of boxed cluster (calibrations as in panel *c*). Bottom: Intracluster interval duration histograms. Solid lines were calculated from the rate constants: $f_2 = 11{,}880\ s^{-1}$, $b_2 = 1880\ s^{-1}$ ($E_2 = 6.3$). For this mutant, $i_0/i_B = 9.2\ pA/4.3\ pA = 2.14$, so the block-corrected values (see Materials and Methods) are $b_2 = 4030$ and $E_2 = 3.0$. On average (Table S1), the E24′I mutation reduced E_2 by 13.8-fold. (*b*) K_d estimation. Left: Clusters elicited by different ACh concentrations. Right: Corresponding interval duration histograms. Solid lines were calculated from a two- (equivalent) site binding scheme: $k_+ = 178 \pm 10\ \mu M^{-1}s^{-1}$ and $k_- = 24{,}548 \pm 1615\ s^{-1}$ (mean ± SD; $K_d = 138 \pm 18\ \mu M$). (*c*) Estimation of the unliganded gating equilibrium constant (E_0). Left: Clusters from a triple-mutant background, without any agonist (boxed cluster expanded, below). The solid lines were calculated from the rate constants using a $C \leftrightarrow O_1 \leftrightarrow O_2$ scheme: $k_{C\leftrightarrow O1} = 840 s^{-1}$, $k_{O1\leftrightarrow C} = 3290\ s^{-1}$; $E_0^{background} = 0.25$. Right: Clusters from E24′I expressed on the triple-mutant background, without any agonist (boxed cluster expanded, below). The probability densities (*solid lines*) were calculated from the rate constants using a $C \leftrightarrow O_1 \leftrightarrow O_2$ scheme: $k_{C\leftrightarrow O1} = 210\ s^{-1}$, $k_{O1\leftrightarrow C} = 10{,}790\ s^{-1}$; $E_0^{E24'I+background} = 0.019$. The E24′I mutation reduced E_0 by 13.1-fold On average the E24′I mutation reduced E_0 and E_2 to approximately the same extents. The results indicate that this mutation does not alter ACh binding to either the **C** or the **O** conformation.

''large'' (5′, 9′, 12′, 13′, and 16′) and four were isoenergetic (2′, 4′, 6′, and 15′). All five ''large'' positions are on the luminal face of εM2, as are the 2′ and 6′ isoenergetic positions. This pattern was similar, but not identical, in the α- and δ-subunits. Considering both α-subunits combined (twice the value shown in Fig. 1), the three ''large'' positions are on the luminal face (9′, 12′, and 13′), and 2′ and 6′ were isoenergetic. In δ, where M2 has only partially been scanned, the luminal positions 12′ and 13′ were ''large'', and 2′ was isoenergetic (6′ of the δ subunit has not been probed). What is common between the luminal residues of M2 at and below 17′ in α, ε, and δ is that, on average, large gating free-energy changes occur at 12′ and 13′ (4.8 ± 0.3 kcal/mol; mean ± SD), somewhat smaller energy changes occur at 9′, 16′, and 17′ (3.1 ± 0.3 kcal/mol), and little or no energy changes occur at 2′ and 6′ (0.9 ± 0.2 kcal/mol).

Fig. 6 (*right*) compares the relative timing of these energy changes, as revealed by the parameter Φ. At this juncture we only consider the timing of the energy changes of residues with ''large'' and ''intermediate'' range-energy values ($n = 8$ in ε, 10 in α, and 3 in δ). There was a bimodal distribution in Φ for these 21 positions (0.58 ± 0.07 and 0.31 ± 0.04), with a tendency for the ''late'' Φ population to have a ''large'' energy range. This suggests that residues exhibiting large gating energy changes tend to experience their **TP** energy change after those exhibiting intermediate range-energy changes. Five of the six 12′ and 13′ residues in α, δ, and ε are ''large and late''.

We now attempt to interpret these M2 patterns of range-energy and Φ with what is known about the structure of this helix in AChRs. One problem with this endeavor is that it is not possible to definitively relate a crystal structure with a functional state of our experiments. Neither the permeability of the pore nor the degree of ligation ensures that a crystal structure will correspond to either the **C** or **O** state that we probe by using kinetics. Another problem is that changes in

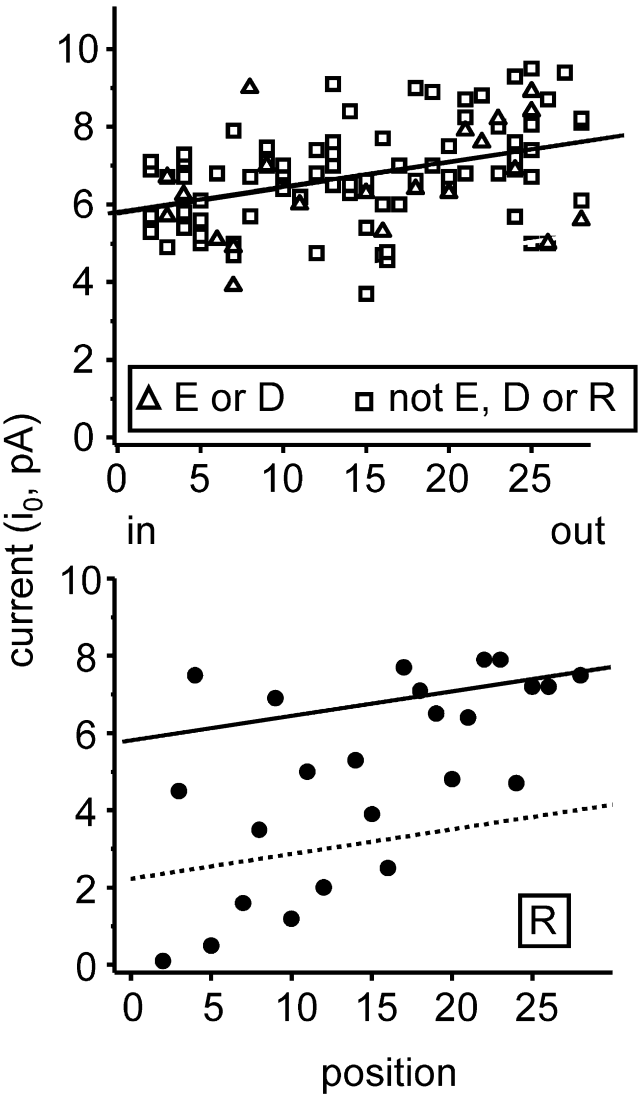

FIGURE 5 Single-channel current amplitudes for εM2 mutants. Current amplitudes elicited by 30 μM ACh (i_0) at +70 mV pipette potential. Top: Nonarginine substitutions. Triangles, E and D; squares, all others. Solid line is the linear fit. Bottom: Arginine substitutions. Solid line as above; the dashed line represents an amplitude that is 3 SD (nonarginine results only) below the solid line. An R side chain at 2′, 5′, 7′, 10′, 12′, and 16′ attenuated the current amplitude significantly.

atomic position mainly suggest changes in enthalpy, whereas kinetic measurements reflect the free energy of the whole system and, hence, both enthalpy and entropy.

The ''gate'' of a channel can be defined as a discrete or distributed region that 1), is the main energetic barrier to ion permeation in the **C** conformation; and 2), moves (changes structure or dynamics) near the end of the **C**→**O** channel-opening process to permit ions to flow rapidly. In ELIC there is a discrete barrier to ion permeation at the bottom of the extracellular aqueous compartment, formed by F16′ in close contact with Y17′ of the adjacent subunit (6). In GLIC and nAChR-*Tm*, the side chains at these two positions do not project into the pore and do not appear to be a barrier to ion flow. In many regards (e.g., with regard to the diameter of the pore at 16′, the orientation of the 16′–17′ side chains, and the tangential and radial tilts of the helix), the structure of M2 in nAChR-*Tm* resembles GLIC more than ELIC.

The question arises: Is the 16′–17′ barrier in ELIC something that is associated with **C**↔**O** gating in AChRs? If so, then we postulate that the unliganded nAChR-*Tm* shape is *not* **C**, but rather **O** (if it can conduct ions (34)), desensitized (if it cannot (35)), or something else. In this case, our experimental results indicate that the **C**→**O** structural change at this discrete gate is not the largest or final energetic event in the **C**→**O** isomerization process. If, however, the 16′–17′ gate of ELIC does not pertain to AChR gating (or perhaps is a structure that prohibits conductance in a conformation other than **C**), then our results suggest that the movement of a distributed M2 region, approximately between 9′ and 13′, serves to switch the flow of ions on and off, as suggested by molecular-dynamics simulations of ion permeation using the nAChR-*Tm* structure (34).

What are the sources of the gating free-energy changes? Regardless of the location and nature of the AChR gate, it is likely that some of the free-energy changes at 9′, 12′, and 13′ arise from protein movements that generate changes in the **C** versus **O** side chains contacts at these positions. The 9′ side chains from all subunits, and the 12′-13′ side chains from adjacent subunits are in closer contact with each other in ELIC compared to GLIC. In addition, in these two proteins the 12′ and 13′ side chains adopt different positions relative to intrasubunit residues in M1 (15′) and M3 (19′). We speculate that some of the **C** versus **O** energy difference at 12′ and 13′ arises from the above changes in atomic positions. Our experiments show that the range-energy values here are smaller in each α-subunit compared to each ε- or δ-subunit. In heteromeric AChRs, the above structural differences would not expected to be strictly symmetric between subunits because the 12′→13′ subunit interaction is α→ε/δ, ε→α or δ→β, and because the M1-15′ side chain is I in ε, β, and δ, but F in α. More experiments are needed to dissect the protein structural components of the energy change at 12′–13′.

Whatever these structural changes in the vicinity of 9′, 12′, and 13′ may be, they do not immediately explain the observation that these residues have low Φ-values and, hence, appear on average to experience their **TP** energy change after 16′–17′. These ''late'' M2 residues appear to be exposed to the pore lumen, and in general the mutations at these positions that increased E_2 (stabilized **O** relative to **C**) were more polar than the WT side chain (Fig. 2). This pattern suggests that the environment around these residues increases in polarity between **C** and **O**. The fact that mutations of the pore-facing 2′ and 6′ positions have little effect on E_2 suggests that the environment around these residues is more or less isoenergetic between **C** and **O** (34,35). Although it is probable that some of the energy change of the ''late'' residues is generated by changes in protein conformation, it is also possible that some of the energy

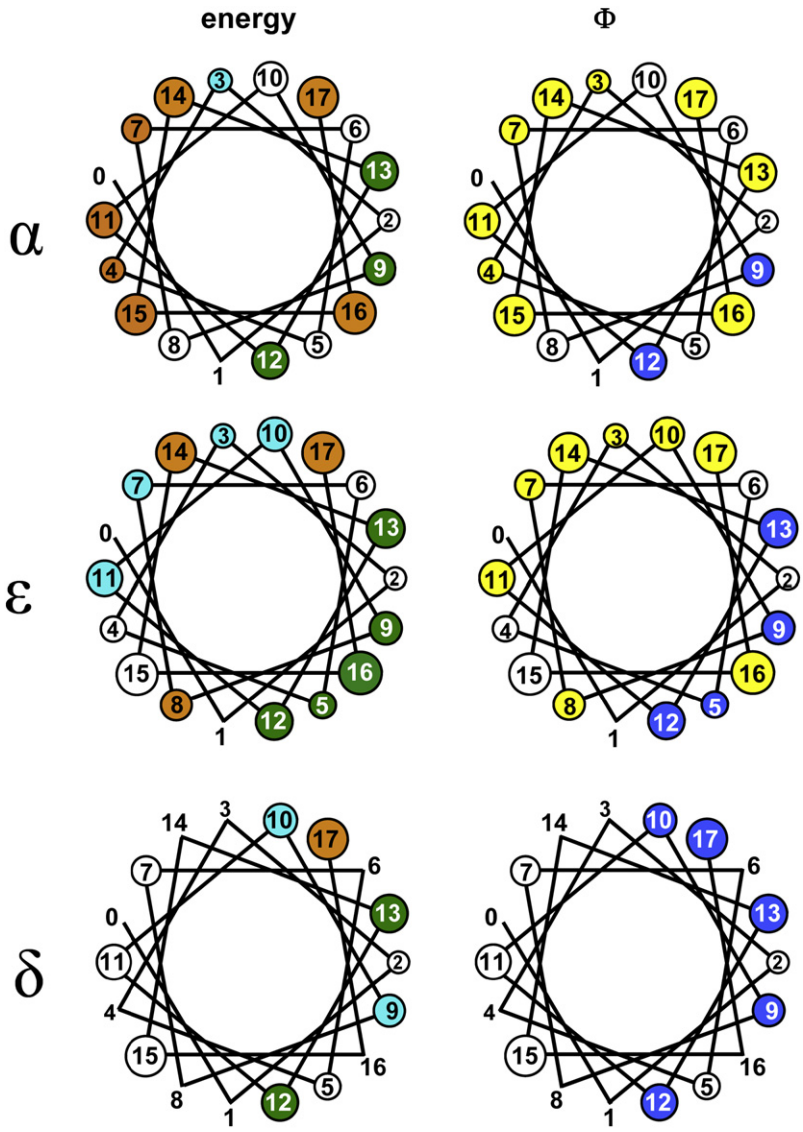

FIGURE 6 Helical wheel representations of range-energy and Φ in M2 ($\leq 17'$) of the α-, ε-, and δ-subunits. The right half ($2'$) of each wheel faces the lumen of the channel; circle size decreases, $17'$–$2'$. Left: Range-energy, derived from the range of E_2 values. Green, >3.8 kcal/mol; orange, 2.5–3.8 kcal/mol; cyan, 1.5–2.5 kcal/mol; white, approximately isoenergetic (<1.5 kcal/mol); no circle, no mutational analysis. Right: Φ (the slope of the R/E plot; see Fig 2). Blue, $\Phi<0.37$; yellow, $0.50<\Phi<0.56$; white, approximately isoenergetic (no Φ estimate); no circle, no mutational analysis. In general, the luminal side chains $9'$, $12'$, and $13'$ experience large energy changes and have low Φ-values.

change is associated with a change in the hydration of this region, which could occur after the tilting movements of M2 and the opening of a discrete gate at $16'$–$17'$ or a distributed gate in the region $9'$–$13'$.

This hypothesis, that a change in the configuration of water contributes to the overall **C** versus **O** energy change, also explains the observation that adjacent residues in M2 can have distinct Φ-values. For example, in εM2 the region $8'$–

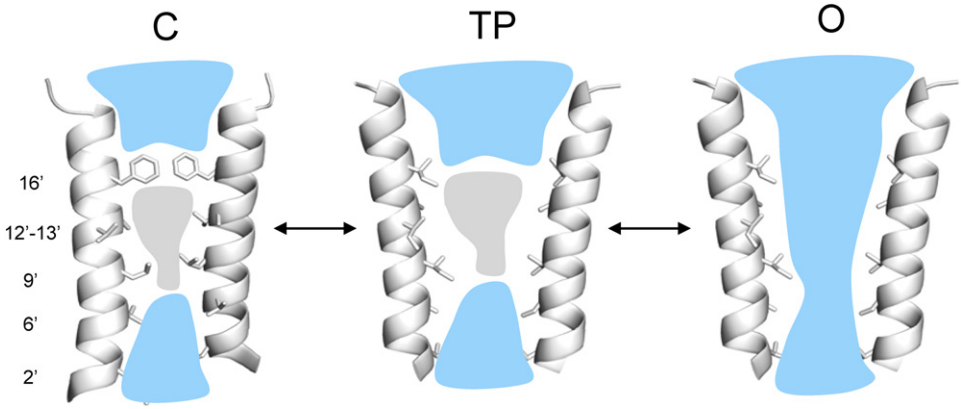

FIGURE 7 A speculative model of M2 gating energy changes. The structures are from ELIC (*left*) and GLIC (*center* and *right* (6,7)). **C**, closed; **TP**, transition pathway; **O**, open. Extracellular ($\geq 16'$) and intracellular ($\leq 6'$) aqueous compartments are blue. The large range-energy values and low Φ-values for the luminal side chains, $9'$–$13'$, could arise from energy changes generated from a combination of changes in protein structure (**C**↔**TP**) and changes in local hydration (**TP**↔**O**).

14′ has the following sequence of Φ: 0.50-**0.37**-0.59-0.55-**0.26**-**0.34**-0.56 (9′, 12′, and 13′, in bold). Such a disjointed pattern might arise from two sequential energy changes occurring within the channel-opening process. The first change would be when the entire M2 helix moves (essentially synchronously) about midway through the **C → O** conformational change. Later, a second energy change would occur when the hydrophobic, pore-facing residues between 9′ and 13′ become more exposed to bulk water. The low experimental Φ-values for just these residues could be weighted averages of the energy change and Φ associated with side-chain motion and a change in hydration (Fig. 7).

We now attempt to synthesize the available experimental findings into a plausible but speculative sequence of events for the channel-opening structural changes in the region of the M2 helices of the AChR. All subunits contribute to a ring of polar residues at position 20′. In the α- (but not ε-) subunit, substantial energy changes occur in this ''cap'' region at the onset of the channel-opening process. We speculate that soon after agonists are bound, the αM2 cap changes energy because of a change in the backbone angles around the central, conserved P23′, a change in the disposition of water in this region, or both (25). These early free-energy changes appear to precede the energy changes in the rest of the αM2 helix, so we postulate that the early movement of the cap contributes to the radial and tangential tilt in the entire helix that leads to the opening of a discrete gate at 16′–17′ or a distributed gate region between 9′ and 13′. This event, in turn, opens the ion permeation pathway, which we imagine as a fusion of the extracellular (>16′) and intracellular (≤6′) aqueous compartments. In the reverse scenario, a spontaneous change in the configuration of water in the equatorial zone precedes and triggers the channel-closing conformational changes in M2.

The M2 gating motions ≤ 17′ appear to be approximately symmetric in the α-, ε-, and δ-subunits. According to the above hypothesis regarding hydration, this pattern suggests that, aside from the αM2-cap domain, both the M2 gating motions and the change in the amount or order of water molecules between 9′ and 13′ occur roughly synchronously and to approximately the same energetic effect, at least in the ε- and α-subunits. There are, however, some exceptions to this symmetry. The Φ-value for most of αM2 (0.63) is slightly greater than for εM2 (0.54). V13′, which has a large range-energy value in α, ε, and δ, has a low Φ-value in ε and δ but not in α. I5′ experiences a large (and late) energy change in ε but not in α or δ. The significance of these M2 asymmetries is, at present, unknown.

SUPPORTING MATERIAL

Two tables and a figure are available at http://www.biophysj.org/biophysj/supplemental/S0006-3495(09)00589-X.

We thank M. Merritt, M. Shero, and M. Teeling for technical assistance, and David Cadugan for helpful discussions.

This work was supported by the National Institutes of Health (NS-23513).

REFERENCES

1. Edelstein, S. J., and J. P. Changeux. 1998. Allosteric transitions of the acetylcholine receptor. *Adv. Protein Chem.* 51:121–184.
2. Sine, S. M., and A. G. Engel. 2006. Recent advances in Cys-loop receptor structure and function. *Nature*. 440:448–455.
3. Changeux, J. P., and A. Taly. 2008. Nicotinic receptors, allosteric proteins and medicine. *Trends Mol. Med.* 14:93–102.
4. Karlin, A. 2002. Emerging structure of the nicotinic acetylcholine receptors. *Nat. Rev. Neurosci.* 3:102–114.
5. Unwin, N. 2005. Refined structure of the nicotinic acetylcholine receptor at 4A resolution. *J. Mol. Biol.* 346:967–989.
6. Hilf, R. J., and R. Dutzler. 2008. X-ray structure of a prokaryotic pentameric ligand-gated ion channel. *Nature*. 452:375–379.
7. Bocquet, N., H. Nury, M. Baaden, C. Le Poupon, J. P. Changeux, et al. 2008. X-ray structure of a pentameric ligand-gated ion channel in an apparently open conformation. *Nature*. 457:111–114.
8. Hilf, R. J., and R. Dutzler. 2009. Structure of a potentially open state of a proton-activated pentameric ligand-gated ion channel. *Nature*. 457: 115–118.
9. Purohit, P. G., and A. Auerbach. 2009. Unliganded gating of acetylcholine receptor channels. *Proc. Natl. Acad. Sci. USA*. 106:115–120.
10. Zhou, Y., J. E. Pearson, and A. Auerbach. 2005. ϕ-Value analysis of a linear, sequential reaction mechanism: theory and application to ion channel gating. *Biophys. J.* 89:3680–3685.
11. Auerbach, A. 2005. Gating of acetylcholine receptor channels: Brownian motion across a broad transition state. *Proc. Natl. Acad. Sci. USA*. 102:1408–1412.
12. Jha, A., D. J. Cadugan, P. Purohit, and A. Auerbach. 2007. Acetylcholine receptor gating at extracellular transmembrane domain interface: the cys-loop and M2–M3 linker. *J. Gen. Physiol.* 130:547–558.
13. Qin, F., A. Auerbach, and F. Sachs. 1997. Maximum likelihood estimation of aggregated Markov processes. *Proc. Biol. Sci.* 264:375–383.
14. Lape, R., D. Colquhoun, and L. G. Sivilotti. 2008. On the nature of partial agonism in the nicotinic receptor superfamily. *Nature*. 454:722–727.
15. Plested, A. J., P. J. Groot-Kormelink, D. Colquhoun, and L. G. Sivilotti. 2007. Single-channel study of the spasmodic mutation α1A52S in recombinant rat glycine receptors. *J. Physiol.* 581:51–73.
16. Elenes, S., and A. Auerbach. 2002. Desensitization of diliganded mouse muscle nicotinic acetylcholine receptor channels. *J. Physiol.* 541:367–383.
17. Colquhoun, D., and A. G. Hawkes. 1981. On the stochastic properties of single ion channels. *Proc. R. Soc. Lond. B*. 211:205–235.
18. Auerbach, A., W. Sigurdson, J. Chen, and G. Akk. 1996. Voltage dependence of mouse acetylcholine receptor gating: different charge movements in di-, mono- and unliganded receptors. *J. Physiol.* 494:155–170.
19. Qin, F. 2004. Restoration of single-channel currents using the segmental k-means method based on hidden Markov modeling. *Biophys. J.* 86: 1488–1501.
20. Auerbach, A., and G. Akk. 1998. Desensitization of mouse nicotinic acetylcholine receptor channels. A two-gate mechanism. *J. Gen. Physiol.* 112:181–197.
21. Purohit, Y., and C. Grosman. 2006. Block of muscle nicotinic receptors by choline suggests that the activation and desensitization gates act as distinct molecular entities. *J. Gen. Physiol.* 127:703–717.
22. Mitra, A., G. D. Cymes, and A. Auerbach. 2005. Dynamics of the acetylcholine receptor pore at the gating transition state. *Proc. Natl. Acad. Sci. USA*. 102:15069–15074.
23. Grosman, C., and A. Auerbach. 2001. The dissociation of acetylcholine from open nicotinic receptor channels. *Proc. Natl. Acad. Sci. USA*. 98:14102–14107.
24. Mitra, A., T. D. Bailey, and A. L. Auerbach. 2004. Structural dynamics of the M4 transmembrane segment during acetylcholine receptor gating. *Structure*. 12:1909–1918.

25. Bafna, P. A., P. G. Purohit, and A. Auerbach. 2008. Gating at the mouth of the acetylcholine receptor channel: energetic consequences of mutations in the αM2-cap. *PLoS ONE*. 3:e2515.

26. Chakrapani, S., and A. Auerbach. 2005. A speed limit for conformational change of an allosteric membrane protein. *Proc. Natl. Acad. Sci. USA*. 102:87–92.

27. Salamone, F. N., M. Zhou, and A. Auerbach. 1999. A re-examination of adult mouse nicotinic acetylcholine receptor channel activation kinetics. *J. Physiol.* 516:315–330.

28. Imoto, K., C. Busch, B. Sakmann, M. Mishina, T. Konno, et al. 1988. Rings of negatively charged amino acids determine the acetylcholine receptor channel conductance. *Nature*. 335:645–648.

29. Wilson, G. G., and A. Karlin. 1998. The location of the gate in the acetylcholine receptor channel. *Neuron*. 20:1269–1281.

30. Cymes, G. D., C. Grosman, and A. Auerbach. 2002. Structure of the transition state of gating in the acetylcholine receptor channel pore: a ϕ-value analysis. *Biochemistry*. 41:5548–5555.

31. Purohit, P., A. Mitra, and A. Auerbach. 2007. A stepwise mechanism for acetylcholine receptor channel gating. *Nature*. 446:930–933.

32. Chakrapani, S., T. D. Bailey, and A. Auerbach. 2004. Gating dynamics of the acetylcholine receptor extracellular domain. *J. Gen. Physiol.* 123: 341–356.

33. Cymes, G. D., Y. Ni, and C. Grosman. 2005. Probing ion-channel pores one proton at a time. *Nature*. 438:975–980.

34. Wang, H. L., X. Cheng, P. Taylor, J. A. McCammon, and S. M. Sine. 2008. Control of cation permeation through the nicotinic receptor channel. *PLOS Comput. Biol*. 4:e41.

35. Beckstein, O., and M. S. Sansom. 2006. A hydrophobic gate in an ion channel: the closed state of the nicotinic acetylcholine receptor. *Phys. Biol.* 3:147–159.